J Appl Electrochem (2014) 44:977–988
DOI 10.1007/s10800-014-0700-4

RESEARCH ARTICLE

Investigation of multilayered quantum dot-sensitized solar cells with different Zn chalcogenide passivation layers

H. K. Jun · M. A. Careem · A. K. Arof

Received: 4 April 2014 / Accepted: 9 June 2014 / Published online: 13 August 2014

Abstract In the case of cadmium sulfide (CdS) and cadmium selenide (CdSe)-based quantum dot-sensitized solar cells (QDSSCs), the addition of a zinc sulfide (ZnS) passivation layer improves the solar cell performance. In this study, multilayered QDSSCs were fabricated using CdS and CdSe quantum dots prepared by successive ionic layer adsorption and reaction (SILAR) method. The optimized QDSSCs were used to study the passivation effect of zinc chalcogenide layers: ZnS, zinc selenide (ZnSe), and zinc telluride (ZnTe). The best performing solar cell prepared from four SILAR cycles of CdS followed by six SILAR cycles of CdSe were used for subsequent deposition of Zn chalcogenide layers. It was observed that capping with ZnSe or ZnTe layer on the multilayered Cd chalcogenide QDs did not improve the solar cell performance. Only the addition of ZnS layer contributed to the better performance of the solar cell. The efficiency obtained in the optimized multilayered CdS/CdSe QDSSC with ZnS layer was 1.37 %, while the QDSSC with ZnSe or ZnTe capping showed lower performance. The behavior of the solar cells is explained with electrochemical impedance spectroscopy study.

Keywords Quantum dot-sensitized solar cell · Zn chalcogenide · Passivation layer · Electrochemical impedance spectroscopy

1 Introduction

Quantum dot-sensitized solar cells (QDSSCs) have become one of the widely researched solar cells in recent years [1]. The large interest in this field is due to the good optical properties of the semiconductor quantum dots (QDs) as well as the ease of fabrication of the QDs [2, 3]. Among the semiconductor materials used as QD sensitizers are CdS [4], CdSe [5], Ag_2S [6], $CuInS_2$ [7], and PbS [8]. Lately, perovskite-based solar cell has emerged as a new breakthrough in QDSSCs and dye-sensitized solar cells (DSSCs) field due to its high performance [9].

In order to achieve high solar cell performance, back electron transfer, or recombination at TiO_2/QD/electrolyte interface needs to be minimized [10, 11]. This can be achieved by altering the surface chemistry of the TiO_2/QD surface. To date, the most popular method is the deposition of a passivation layer on the TiO_2/QD surface. ZnS has been proven to be a good passivation layer for minimizing recombination process at the TiO_2/QD/electrolyte interface [12]. Besides ZnS, other organic or inorganic materials can also be applied as a passivation layer although some of the results might not be as good as that with ZnS [13]. In this study, optimized CdS/CdSe QDSSCs were used to study the effect of the Zn chalcogenide (ZnS, ZnSe, or ZnTe) passivation layers. The effect of ZnS was first studied. This

Electronic supplementary material The online version of this article (doi:10.1007/s10800-014-0700-4) contains supplementary material, which is available to authorized users.

H. K. Jun · M. A. Careem · A. K. Arof (✉)
Centre for Ionics University of Malaya (CIUM), Department of Physics, University of Malaya, 50603 Kuala Lumpur, Malaysia
e-mail: akarof@um.edu.my

H. K. Jun
e-mail: junhk1@gmail.com

M. A. Careem
e-mail: macareem@um.edu.my

H. K. Jun
Department of Mechanical and Material Engineering, Universiti Tunku Abdul Rahman, Jalan Genting Kelang, 53300 Kuala Lumpur, Malaysia

was followed by assessment on the suitability of other Zn chalcogenide materials (ZnSe and ZnTe) as the passivation layer instead of ZnS. To the authors' best knowledge, there is no report in the literature on the performance of ZnSe and ZnTe as the passivation layers in QDSSCs.

2 Experimental

2.1 Materials

Titanium dioxide (TiO_2) paste (18NR) was obtained from JGC C&C, Japan. Fluorine-doped tin oxide (FTO) conducting glasses (8 Ω sq^{-1} sheet resistance) purchased from Solaronix, Switzerland were used for the preparation of the electrodes. TiO_2 compact layer was prepared from 0.38 M ethanolic solution of di-isopropoxytitanum bis(acetylacetonate) (Sigma-Aldrich). Cadmium nitrate tetrahydrate, selenium dioxide, sodium borohydride, sulfur, and guanidine thiocyanate (GuSCN) were all purchased from Sigma-Aldrich while sodium sulfide nonahydrate was procured from Bendosen, Germany.

2.2 Preparation of TiO_2 film working electrode

The compact layer of TiO_2 was first prepared by spin coating di-isopropoxytitanum bis(acetylacetonate) solution on the FTO glass substrate surface at 3,000 rpm for 10 s. The coated FTO glass was then sintered at 450 °C for 30 min. The acquired TiO_2 compact layer enhances the adhesion of TiO_2 to the substrate as well as provides a larger TiO_2/FTO contact area ratio. It also helps to minimize electron recombination by reducing the contact between the electrolyte and the glass substrate [14]. TiO_2 paste was then deposited on the glass substrate using doctor blade method. The newly deposited layer was sintered at 450 °C for 30 min in order to remove any organic residues and moisture and to obtain a mesoporous TiO_2 layer.

2.3 Fabrication of CdS/CdSe QD-sensitized electrodes

Both CdS and CdSe QDs were prepared using successive ionic layer adsorption and reaction (SILAR) deposition method. To fabricate CdS QDs, a TiO_2-coated electrode was successively dipped into 0.1 M $Cd(NO_3)_2$ ethanol solution for 5 min and 0.1 M Na_2S methanol solution for 5 min. The electrode was rinsed with alcohol and allowed to dry in between the dipping process. This two-step dipping is termed as 1 SILAR cycle.

For CdSe QDs, preparation process was performed in a glove box filled with argon gas following the literature procedure [15]. A TiO_2-coated electrode was dipped into 0.03 M $Cd(NO_3)_2$ ethanol solution for 30 s followed by ethanol rinsing and drying. Then it was dipped into Se^{2-} solution for 30 s followed by ethanol rinsing and drying. Se^{2-} solution was prepared by reacting 0.03 M SeO_2 ethanolic solution with 0.06 M $NaBH_4$. The mixture was stirred for about an hour before it was used for SILAR dipping process. For the preparation of ZnS layer on the QD-coated TiO_2 surface, the SILAR dipping was performed in $Zn(CH_3COO)_2$ ethanol solution and Na_2S methanol solution. The dipping time in each solution is 1 min. Meanwhile for ZnSe layer, the same procedure as in the preparation of CdSe QDs with cationic solution replaced with $Zn(NO_3)_2$ was followed. For ZnTe layer, TeO_2 was used to react with $NaBH_4$ instead of SeO_2. The QDs prepared are referred to as CdS(n) and CdSe(n), respectively, where n is the number of SILAR cycles used for preparing them.

2.4 Assembly of QDSSCs

Solar cell was fabricated by clamping the QD-sensitized TiO_2 electrode with a platinized counter electrode. Platinum electrode was prepared by spin coating a thin layer of Plastisol solution (Solaronix, Switzerland) on the conducting glass surface. The electrode was then sintered at 450 °C for 30 min.

Parafilm (130 μm thickness) was used as a spacer between the two electrodes. It prevented the electrolyte from leaking. Droplets of the polysulfide electrolyte were dropped onto the surface of QD-sensitized TiO_2 film until full coverage was obtained prior to the cell assembly. The effective working area of the QD-sensitized TiO_2 film was 0.25 cm^2. The polysulfide electrolyte solution for the QDSSC was prepared from 0.5 M Na_2S, 0.1 M S, and 0.05 M GuSCN in water/ethanol = 2:8 (v:v) [16].

2.5 Photoresponse measurement and characterizations

Photocurrent–voltage (I–V) characteristics of the QDSSCs were measured using a Keithley 2400 electrometer under illumination from a xenon lamp at the intensity of 1,000 W m^{-2}. Efficiency was calculated from the equation

$$\eta = \frac{Jsc \times Voc \times FF}{P_{in}}, \quad (1)$$

where J_{SC} is the photocurrent density measured at short-circuit, V_{OC} is open-circuit voltage, FF is fill factor, and P_{in} is the intensity density of the incident light. Measurement on each cell was repeated three times to ensure the consistency of the data.

Optical characteristics of the QD-sensitized photoelectrodes were carried out with a Shimadzu PC3101 UV–Vis NIR spectrophotometer. Surface morphology of the QD-sensitized electrode was examined with field emission

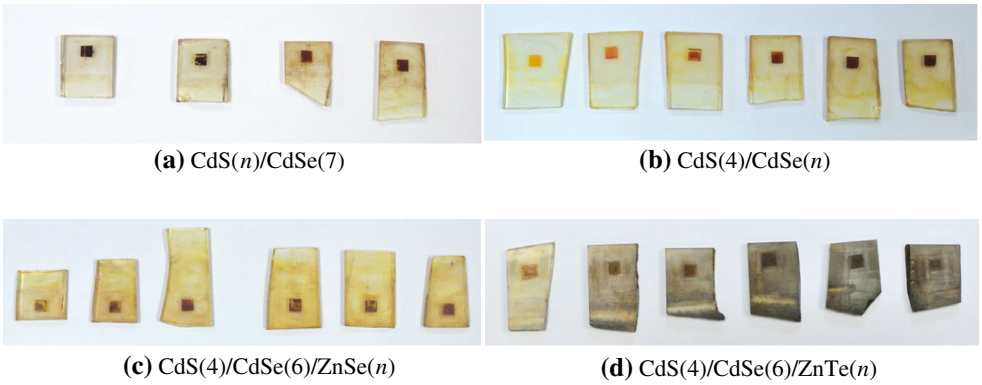

(a) CdS(*n*)/CdSe(7) **(b)** CdS(4)/CdSe(*n*)

(c) CdS(4)/CdSe(6)/ZnSe(*n*) **(d)** CdS(4)/CdSe(6)/ZnTe(*n*)

Fig. 1 The effect of the number of SILAR cycles on the color change of the QD-sensitized TiO_2 layer. *n* is the number of SILAR cycles which increases sequentially from the most left sample to the right sample

scanning electron microscopy (FESEM, Jeol JSM-7600F) and transmission electron microscopy (TEM, Jeol JEM-2100F). Multilayered QD-sensitized TiO_2 film was also analyzed using a distribution mapping technique by energy dispersive X-ray spectroscopy (EDX).

Electrochemical impedance spectroscopy (EIS) study was performed using an Autolab potentiostat/galvanostat. Measurements were performed with cells under dark condition. The cells were biased at the same potential as explained in the result section with a 15 mV RMS voltage perturbation. Frequency range used was 10^6 to 0.01 Hz. EIS results were fitted with *ZSimWin* software to obtain the series resistance and charge-transfer resistance (R_r) at the photoanode/electrolyte interface.

3 Results and discussion

3.1 Surface morphology

SILAR method has been used to prepare QDs for sensitization of TiO_2 due to its simplicity and easy control of the QD size [17, 18]. The TiO_2 thickness has been determined to be around 12 μm as observed from FESEM image (see Fig. S1 in Supplementary material). Mixed QDs were prepared by depositing CdS QDs first followed by CdSe deposition. The passivation layers were then deposited on top of the QD layers. As the SILAR cycles increased, the depth of the color of the QD-sensitized TiO_2 layer increased as shown in Fig. 1.

When the number of CdSe QD depositions was fixed at 7 SILAR cycles, and the number of CdS depositions was changed from 1 to 4 cycles, there is only a slight color change observed as shown in Fig. 1a. This is due to the significantly strong dark color of CdSe(7) layer although there was a gradual increase from light yellow to orange corresponding to CdS(1) to CdS(4). However, when the CdS layer was fixed at 4 SILAR cycles and CdSe layer was varied from 1 to 7 SILAR cycles, the change of color of the QD-sensitized TiO_2 was clearly seen as in Fig. 1b. The color changed from light orange to dark brown. For the CdS(4)/CdSe(7)/ZnSe(*n*) QD-sensitized TiO_2, the color change (Fig. 1c) was not significant compared with that of the CdS(4)/CdSe(7)/ZnTe(*n*) QD-sensitized TiO_2 (Fig. 1d). It was observed that addition of ZnTe layers had more darkening effect compared with that produced by ZnSe layers which only manifested in dark red. The change of the color with different number of SILAR cycles is due to the quantum confinement effect of the QDs which corresponds to the change of the QD size [19, 20]. As the number of SILAR cycles increased, the QD size usually increased until an optimum size is reached and then decreased due to QDs overcrowding effect.

Observation of surface morphology through FESEM revealed that the particle size increased with more deposition of QDs. When the TiO_2 layer is sensitized with CdS and CdSe QDs, the particle size appears slightly larger compared with bare TiO_2 layer (see Fig. 2a, b). Addition of ZnSe and ZnTe layers seem to form a matrix layer on top of the TiO_2/QD particles (Fig. 2c, d). The ZnSe and ZnTe layers look like a barrier which may hinder the electron transfer through the TiO_2 layer (this effect shall be explained in the following sections).

To verify that ZnSe and ZnTe layers had indeed formed on top of CdS/CdSe QDs layers, samples were analyzed via TEM imaging and EDX. TEM images are shown in Fig. 3 while EDX result is shown in Fig. 4. It was observed that CdS QDs formed as the underlayer on the TiO_2 particles. This is followed by CdSe QDs forming on top of CdS QDs. Finally, both ZnSe and ZnTe layers appear as thin layers on top of CdS or CdSe QDs. The absence of ZnTe on the bare TiO_2 particles suggests that ZnTe passivation layer may require a QD underlayer for seed growth or the growth on TiO_2 particle maybe specific on certain crystallographic

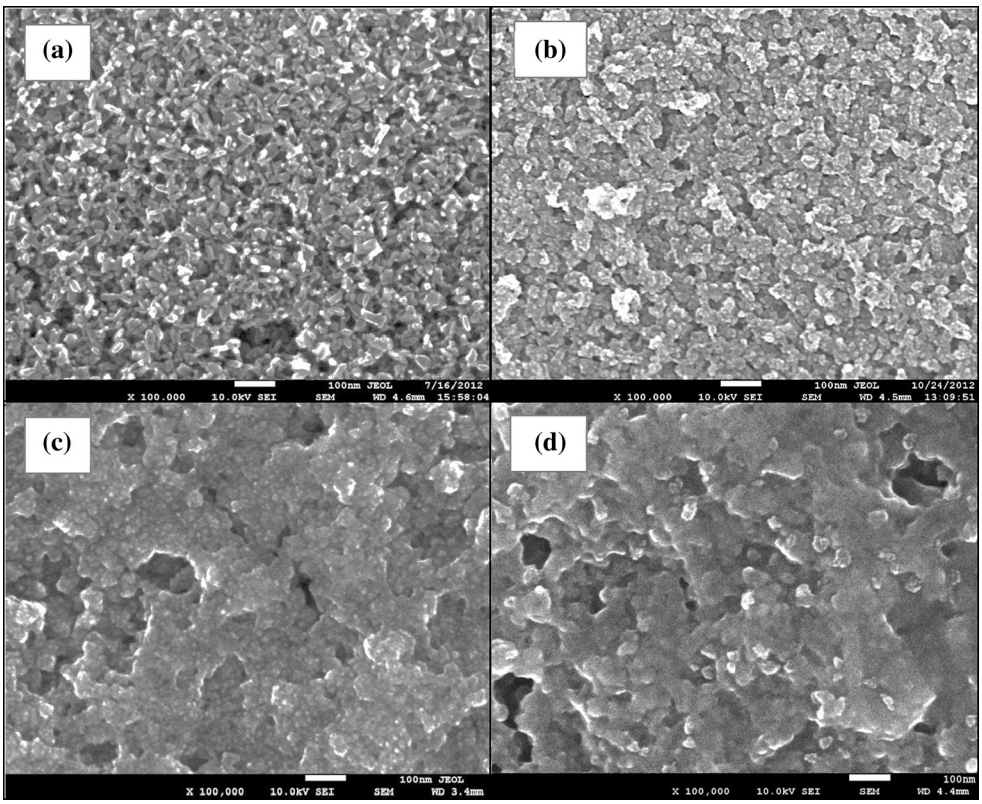

Fig. 2 FESEM images of **a** bare TiO_2, **b** CdS(4)/CdSe(6)—sensitized TiO_2, **c** CdS(4)/CdSe(6)/ZnSe(6)—sensitized TiO_2, and **d** CdS(4)/CdSe(6)/ZnTe(6)—sensitized TiO_2. All images are shown with ×100,000 magnification

planes. Furthermore, ZnTe layer may not be stable and easily degraded upon exposure to air as in the case of CdTe [21]. Nevertheless, EDX result (Fig. 4) indicates that Te element is still present in the sample.

3.2 J–V curves

The performances of the solar cells were measured under illumination. In determining the optimum performance of CdS(*n*)/CdSe(*n*), a series of studies were performed to determine the SILAR cycle required to deposit CdS and CdSe QDs on the TiO_2 electrode. Detailed results were included in supplementary material. To confirm the SILAR cycle required for the deposition of CdS QDs, CdSe QDs layer was deposited at 7 SILAR cycles based on previous study [22]. UV–Vis spectroscopy results on this batch of cells indicate that the absorption edges of the 4 photoanodes do not differ much, which is at around 650 nm (see Fig. S2). Therefore, it is expected that the solar cell performance may not vary much. However, the actual performances do not adhere with the UV–Vis spectra result (see Fig. S3; Table S1). CdS(4)/CdSe(7) QDSSC has the best performance. This indicates that the addition of CdS QD underlayer helps to enhance the solar cell performance. In this study, the number of SILAR cycles for CdS deposition was limited to 4 considering the optimum performance was obtained with CdS(4) QDSSC.

With the CdS QDs layer deposited at 4 SILAR cycles, increasing the number of SILAR cycle for CdSe QDs deposition resulted in the increase of absorbance intensity of the electrodes (Fig. S4). However, the absorption edges of the cells only change slightly, within the range of 625–675 nm. Nevertheless, there is a reduction of effective bandgap energy which suggests a red-shift effect. For low bandgap energy, the estimated effective QD diameter will be large as in the case of CdS(4)/CdSe(6)-sensitized TiO_2 film. The shifting of the absorption edge with the number of SILAR cycles for CdSe deposition indicates the tunability of the effective bandgap energy of the QDs. In terms of solar cell performance, CdS(4)/CdSe(6) QDSSC gives the highest efficiency among the cells as shown in Fig. S5 and Table S2. This efficiency is higher than that of the previous cell in the CdS(*n*)/CdSe(7) QDSSC batch and is slightly better than the reported result of 1.06 % [23]. However, it is also lower than other reported result which is above 1.50 % [24, 25]. We think that the difference could be attributed to the QDs growing process during the SILAR process as a longer time for rinsing and drying is beneficial. As a result, distribution of QDs could be inhomogeneous within the TiO_2 layer [26]. The better photocurrent

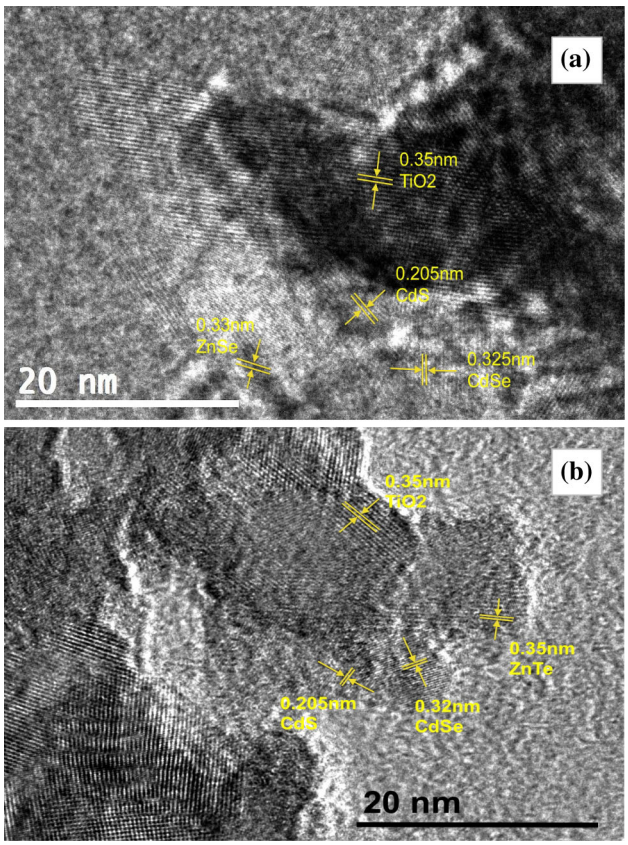

Fig. 3 TEM images of **a** CdS(4)/CdSe(6)/ZnSe(6)—sensitized TiO_2, **b** CdS(4)/CdSe(6)/ZnTe(6)—sensitized TiO_2

injection in that cell with CdS(4)/CdSe(6) sensitized TiO_2 film is attributed to the well alignment of the energy band positions of CdS(4)/CdSe(6) cascade structure [27, 28]. However, as more CdSe QD layers were deposited, the cell performance started to deteriorate that maybe due to the overcrowding of QDs which would slow down the charge transfer from the QDs to the TiO_2 and substrate. The same effect was also observed in Zhang et al.'s [24] work in which more QDs deposition had detrimental effect on the generation and collection of the charges. It is also observed that the performance of CdSe(7) QDSSC does not differ much with CdS(4)/CdSe(7) QDSSC which indicates the redundancy of CdS underlayer in the multilayered structure [29]. Nevertheless, this only applies when the CdSe is deposited using more than six SILAR cycles, as in our case the performance of CdSe(6) QDSSC (result not shown here) is inferior to those of CdSe(7) and CdS(4)/CdSe(6) QDSSCs.

ZnS layer deposited on top of CdS/CdSe layer has proven to bring positive effect on the cell performance similar to the effects as observed in single CdS or CdSe QDSSC [12, 25, 27, 30, 31]. In this study, the best performing co-sensitized cell with CdS(4)/CdSe(6) QDs structure was used to study the effect of an additional ZnS layer. The deposition of ZnS was made using two SILAR cycles only based on the literature [12, 25]. As seen in Fig. 5 and Table 1, the addition of ZnS layer has improved the photocurrent density and increased the efficiency by 22 %.

On the other hand, if the ZnS layer was substituted with other Zn chalcogenide layers such as ZnSe and ZnTe, it was expected that the cell performance should improve as well. In the next study, ZnSe layer was deposited on top of CdS(4)/CdSe(6)-sensitized TiO_2 film using 1–6 SILAR cycles. The corresponding solar cells performances are shown in Fig. 6 and their performance parameters are tabulated in Table 2. With the ZnSe as passivation layer on QD-sensitized TiO_2 film, the cell performance is found to decrease compared to that of the cell having ZnS as passivation layer. The major effect of the addition of ZnSe is the decrease of the open-circuit voltage. As the number of SILAR cycles for ZnSe deposition increased, the efficiency of the solar cell is increased as well. This effect is largely assigned to the photocurrent density trend. Photocurrent density increased in tandem with more SILAR cycles of ZnSe deposition except for CdS(4)/CdSe(6)/ZnSe(2) QDSSC. The slightly higher value of photocurrent density in this solar cell could be attributed to the faster charge injection in QDs owing to better band energy alignment of the cascade CdS(4)/CdSe(6)/ZnSe(2) structure. In general, more ZnSe deposition should contribute to the improvement of charge injection as it has a bandgap energy of 2.7 eV. The low bandgap energy of ZnSe compared to ZnS implies that ZnSe could take part in the photocurrent transportation instead of functioning as a passivation layer. This phenomenon was supported by UV–Vis spectrum of the batch as shown in Fig. 7, where an increase of absorbance intensity comes with the red-shift of the spectra as ZnSe layers increased. On the other hand, the overall low open-circuit voltage indicates slow hole reduction from the QD to the electrolyte. Perhaps a better performance can be expected with a better redox mediator. The highest performance is obtained when ZnSe was deposited with 6 SILAR cycles. We expect the efficiency could go even higher with a few more SILAR cycles. However, with more deposition of ZnSe QDs, QD overcrowding may affect the performance of the solar cells.

In the following study, ZnTe layer was deposited on CdS(4)/CdSe(6) QD-sensitized TiO_2 film with SILAR cycles ranging from 1 to 6. The J–V curves of the cells are shown in Fig. 8 while Table 3 lists the performance parameters of the cells. From the results, it can be seen that the efficiency of the cells decreased with the increasing number of SILAR cycles used for the deposition of ZnTe. The highest performance was obtained in CdS(4)/CdSe(6)/ZnTe(1) QDSSC with an efficiency of 0.90 %. This result is similar to that obtained for CdSe(7) QDSSC indicating

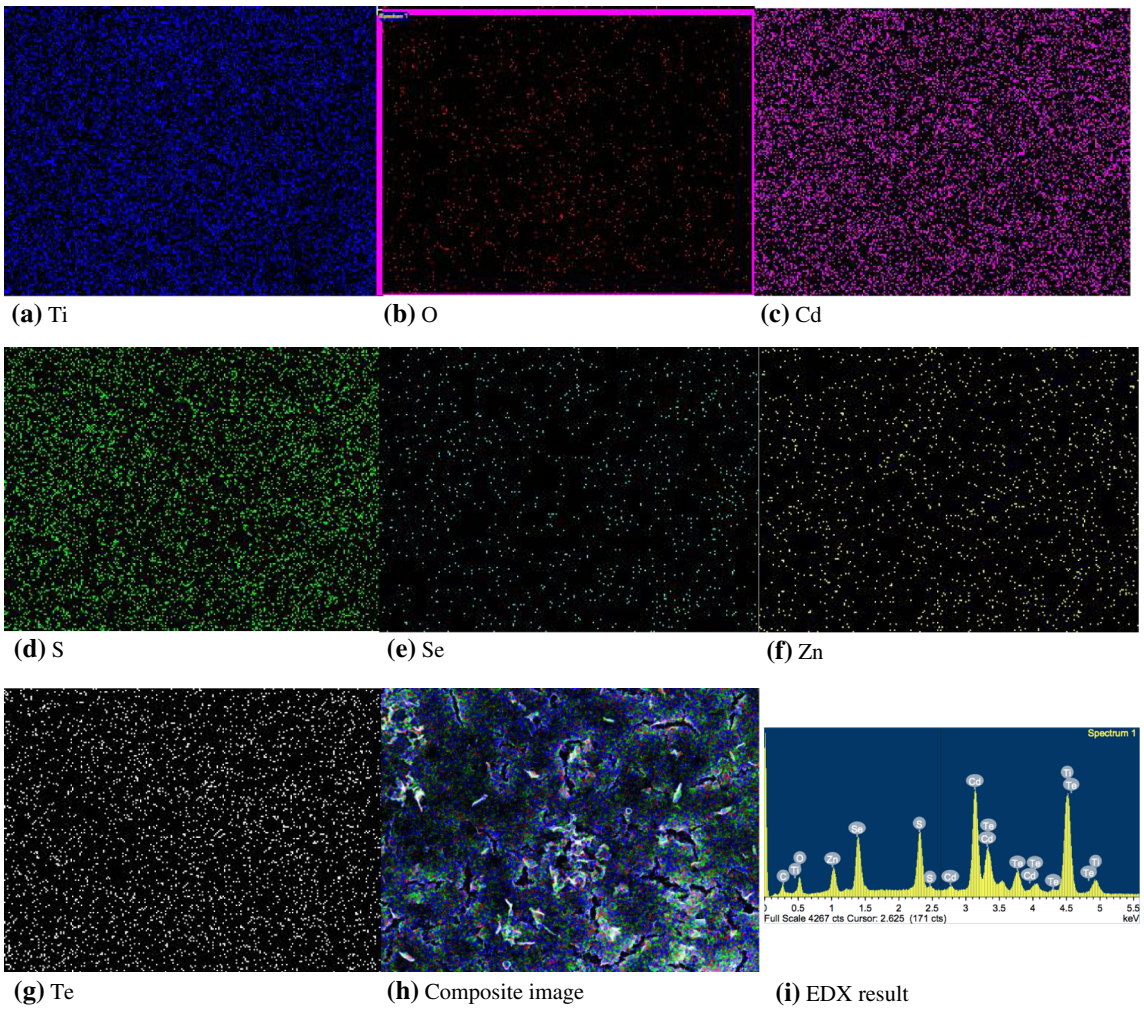

Fig. 4 EDX mapping analysis of CdS(4)/CdSe(6)/ZnTe(6)—sensitized TiO_2 sample

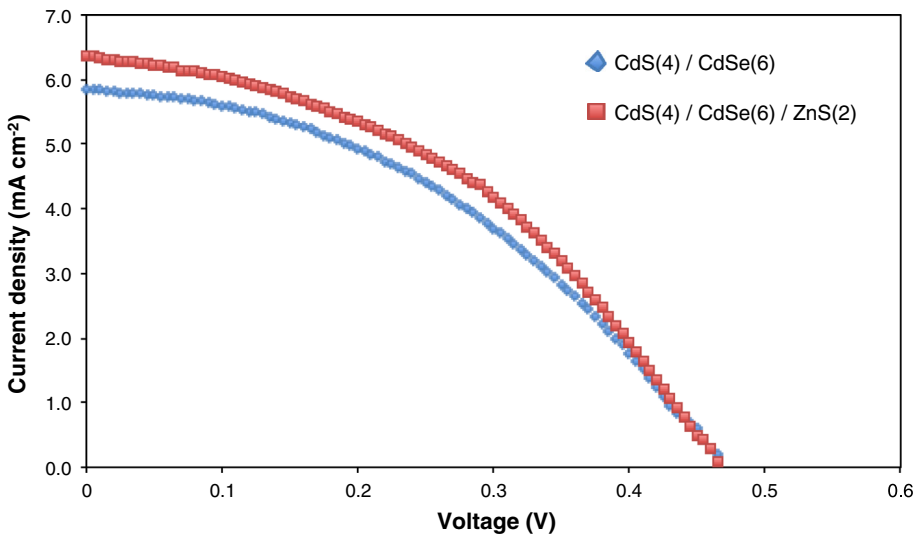

Fig. 5 J–V curves of CdS(4)/CdSe(6) QDSSCs with and without ZnS layer

Table 1 Performance parameters of CdS(4)/CdSe(6) QDSSCs with and without ZnS layer

Sample	J_{sc} (mA cm^{-2})	V_{OC} (V)	FF (%)	η (%)
CdS(4)/CdSe(6)	5.85	0.465	41	1.12
CdS(4)/CdSe(6)/ ZnS(2)	6.37	0.465	45	1.37

Table 2 Performance parameters of CdS(4)/CdSe(6)/ZnSe(n) QDSSCs

Sample	J_{sc} (mA cm^{-2})	V_{OC} (V)	FF (%)	η (%)
CdS(4)/CdSe(6)/ ZnSe(1)	3.32	0.335	32	0.36
CdS(4)/CdSe(6)/ ZnSe(2)	6.06	0.345	33	0.69
CdS(4)/CdSe(6)/ ZnSe(3)	3.86	0.425	42	0.69
CdS(4)/CdSe(6)/ ZnSe(4)	4.21	0.385	34	0.55
CdS(4)/CdSe(6)/ ZnSe(5)	5.26	0.380	36	0.72
CdS(4)/CdSe(6)/ ZnSe(6)	5.82	0.420	44	1.08

the redundancy of ZnTe layer. In fact, the more SILAR cycles used for the deposition of ZnTe, the more deterioration of the cell performance would be. The decrease of the photocurrent density with more ZnTe layers shows the negative effect on charge injection with the addition of ZnTe layer. However, the open-circuit voltage of the batch is higher compared with that of the previous batch of CdS(4)/CdSe(6)/ZnSe(n) QDSSCs. This result shows that ZnTe layers may not be suitable to be applied as a passivation layer in QDSSCs. The negative effect of the cells with ZnTe layer could be due to energy band misalignment within the cascade structure of CdS(4)/CdSe(6)/ZnTe(n).

3.3 EIS measurements

The behavior of QDSSC is also investigated using EIS. A typical EIS spectrum consists of three semicircles in the Nyquist plot [32, 33]. The three semicircles correspond to the response in high-frequency, intermediate-frequency, and low-frequency regions under normal open-circuit potential bias. Response in the high-frequency region is attributed to the charge transfer between the electrolyte and counter electrode interface while the intermediate-frequency response indicates the charge transport in the QD-sensitized TiO_2 layer and the recombination process at the QD-sensitized TiO_2/electrolyte interface. Finally, the low-frequency response revolves on the diffusion process in the electrolyte. Most of the time, only a double arc is observed for a low performance QDSSC in which the feature of electrolyte diffusion is rarely present. In our study, we applied the transmission line model for the curve fitting [34]. The equivalent circuit of QDSSC in a conductive state comprises a combination of a series resistance and two time constant elements. As all the QDSSCs had the same liquid electrolyte and counter electrode material, the resistance and impedance at counter electrode/electrolyte interface should not differ much. The variation in the series resistance could be due to difference in the surface roughness and thickness of the compact layer and counter electrode.

Figure 9 shows the Nyquist plots of CdS(n)/CdSe(7) QDSSC batch. The corresponding resistance and impedance data are tabulated in Table 4. All the cells in this batch were measured at 0.45 V potential bias under dark condition. The series resistances of the cells lie between the

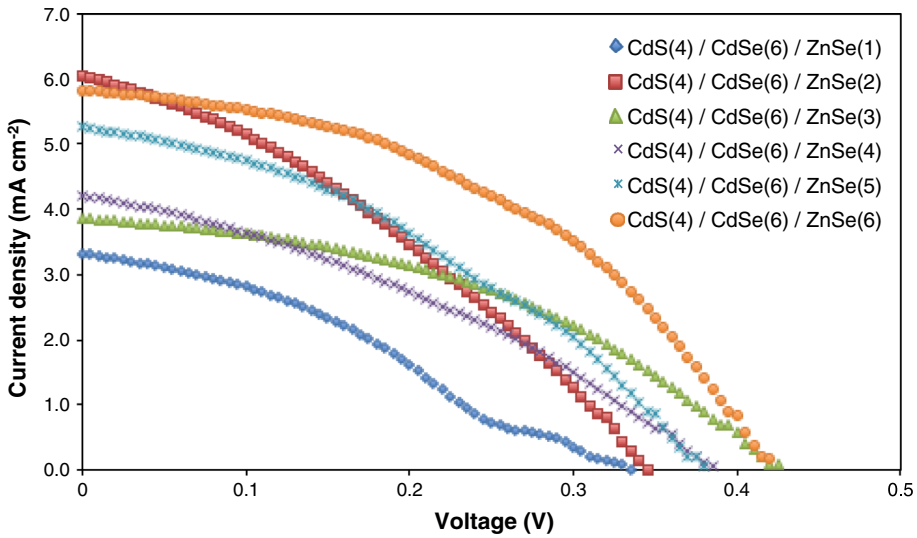

Fig. 6 J–V curves of CdS(4)/CdSe(6)/ZnSe(n) QDSSCs

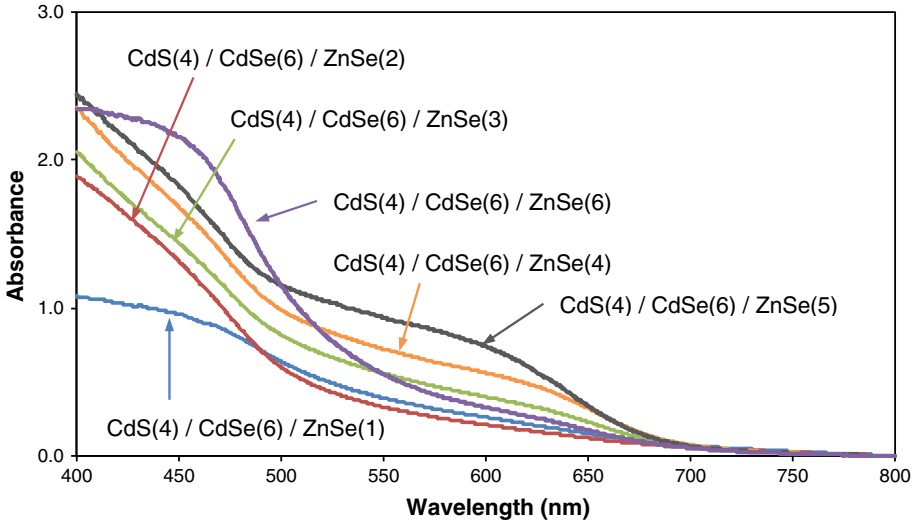

Fig. 7 UV–Vis spectra for CdS(4)/CdSe(6)/ZnSe(*n*)—sensitized TiO_2 where *n* changes from 1 to 6

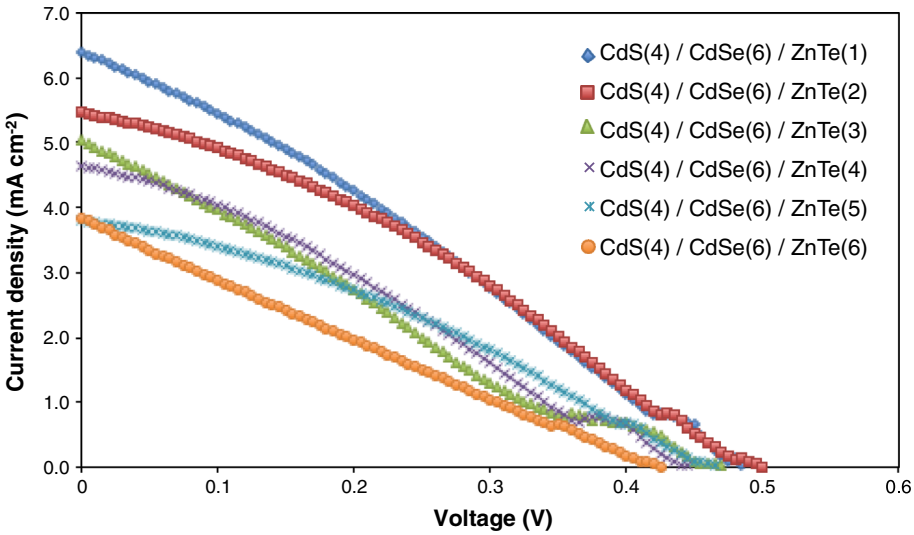

Fig. 8 J–V curves of CdS(4)/CdSe(6)/ZnTe(*n*) QDSSCs

Table 3 Performance parameters of CdS(4)/CdSe(6)/ZnTe(*n*) QDSSCs

Sample	J_{sc} (mA cm^{-2})	V_{OC} (V)	FF (%)	η (%)
CdS(4)/CdSe(6)/ZnTe(1)	6.39	0.485	29	0.90
CdS(4)/CdSe(6)/ZnTe(2)	5.46	0.500	32	0.87
CdS(4)/CdSe(6)/ZnTe(3)	5.03	0.470	23	0.54
CdS(4)/CdSe(6)/ZnTe(4)	4.64	0.445	29	0.60
CdS(4)/CdSe(6)/ZnTe(5)	3.80	0.465	33	0.58
CdS(4)/CdSe(6)/ZnTe(6)	3.84	0.425	24	0.39

range of 30–40 Ω. If a highly conductive material is used as the counter electrode such as Cu_2S, the series resistance is expected to reduce [35]. The charge-transfer resistances at photoanode/electrolyte interface, R_r of the batch do not vary much. R_r is also related to recombination of electrons at the photoanode/electrolyte interface. In the events of low recombination, the charge-transfer resistance is generally higher than the electron transport resistance within the photoanode [34]. On the other hand, the true chemical capacitance, C_μ increases with increasing number of SILAR cycles used for the CdS QDs. Consequently, the electron lifetime of the cells is increased with higher number of SILAR cycles of CdS QD indicating a slower recombination rate of the electron at that interface. This result correlates with the efficiency result obtained from J–V curves as in the case of CdS(4)/CdSe(7) QDSSC. The

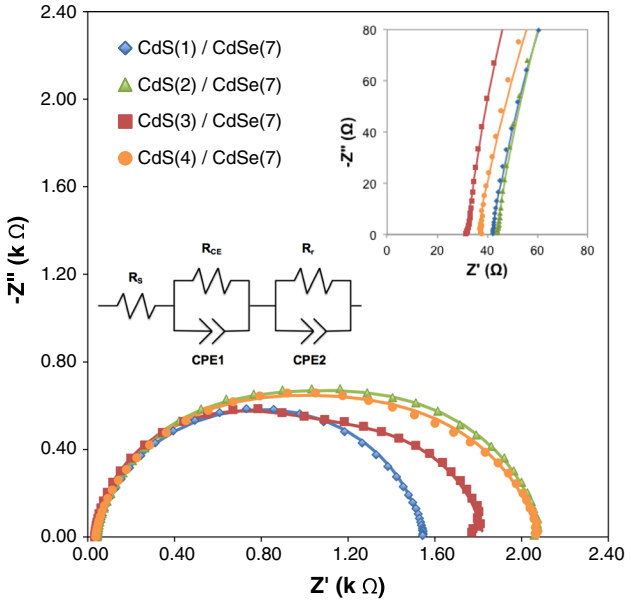

Fig. 9 Nyquist plots of CdS(*n*)/CdSe(7) QDSSCs in dark with 0.45 V bias. The equivalent circuit of the QDSSC with the representation of series resistance (subscript s), impedance at QD-sensitized TiO_2/electrolyte (subscript r), and counter electrode/electrolyte interface (subscript CE). The symbol *R* and CPE denote the resistance and constant phase element, respectively. Details of the plot at high frequencies are shown in the *inset*

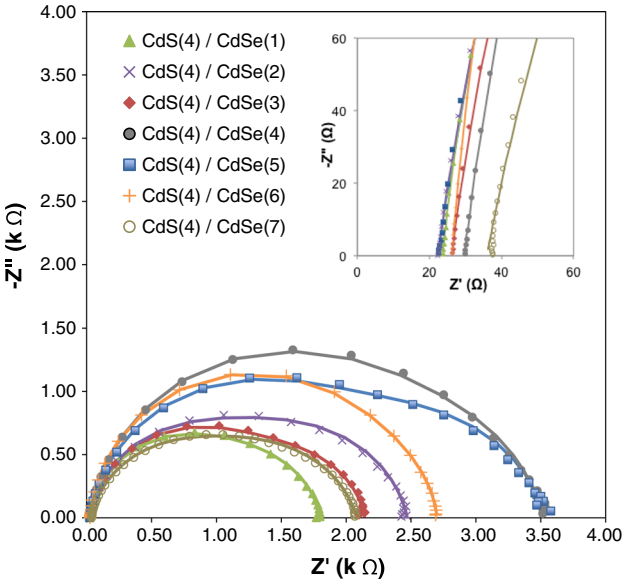

Fig. 10 Nyquist plots of CdS(4)/CdSe(*n*) QDSSCs in dark with 0.45 V bias. Details of the plots at high frequencies are shown in the *inset*

Table 4 EIS results of CdS(*n*)/CdSe(7) QDSSCs in dark with 0.45 V bias: series resistance, charge-transfer resistance, impedance, and electron lifetime

Sample	R_S (Ω)	R_r (kΩ)	CPE2-T (μS s^n)	CPE2-P ($0 < n < 1$)	τ (ms)
CdS(1)/CdSe(7)	41.68	0.97	15.90	0.88	8.93
CdS(2)/CdSe(7)	43.61	1.15	31.22	0.87	21.92
CdS(3)/CdSe(7)	31.96	0.82	61.72	0.88	33.63
CdS(4)/CdSe(7)	35.90	0.92	69.66	0.90	46.46

electron lifetime, τ was calculated using Eq. (2) by incorporating the true chemical capacitance value [36].

$$\tau = R_r C_\mu, \tag{2}$$

$$\tau = [(\mathrm{CPE} - T) \times R_r]^{1/n}. \tag{3}$$

A higher value of τ is favorable as electron recombination is delayed at the photoanode/electrolyte interface.

For the batch of CdS(4)/CdSe(*n*) QDSSCs, the Nyquist plots are shown in Fig. 10 and the EIS data are presented in Table 5. The samples were measured at 0.45 V potential bias under dark. Compared with the previous batch of cells, the charge-transfer resistance, R_r appears to be slightly higher on average. This increase is due to the additional CdSe QDs which can produce additional resistance to the charge transfer pathway. Similarly, the true chemical capacitance is increased with increasing number of SILAR cycles of CdSe QD. However, as the optimum performance is in CdS(4)/CdSe(6) QDSSC, the true chemical capacitance value begins to reduce with more CdSe QD layers. The electron lifetime of the samples correlates well with the performance of the solar cell. The longest electron

Table 5 EIS results of CdS(4)/CdSe(*n*) QDSSCs in dark with 0.45 V bias: series resistance, charge-transfer resistance, impedance, and electron lifetime

Sample	R_S (Ω)	R_r (kΩ)	CPE2-T (μS s^n)	CPE2-P ($0 < n < 1$)	τ (ms)
CdS(4)/CdSe(1)	23.61	1.10	3.72	0.94	2.84
CdS(4)/CdSe(2)	22.20	1.07	6.61	0.93	4.82
CdS(4)/CdSe(3)	26.11	0.82	46.91	0.89	25.44
CdS(4)/CdSe(4)	29.62	1.00	58.17	0.88	38.75
CdS(4)/CdSe(5)	22.27	1.56	65.43	0.84	66.45
CdS(4)/CdSe(6)	26.23	1.27	66.78	0.95	74.87
CdS(4)/CdSe(7)	35.90	0.92	69.66	0.90	46.46

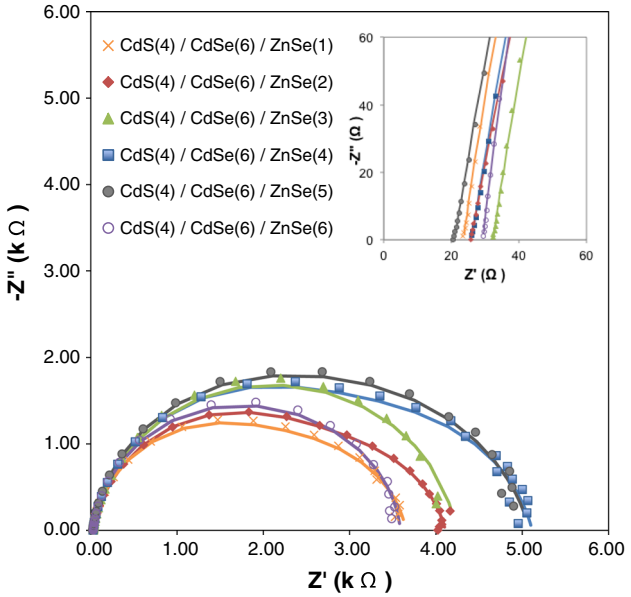

Fig. 11 Nyquist plots of CdS(4)/CdSe(6)/ZnSe(n) QDSSCs under dark with 0.40 V bias. Details of the plots at high frequencies are shown in the *inset*

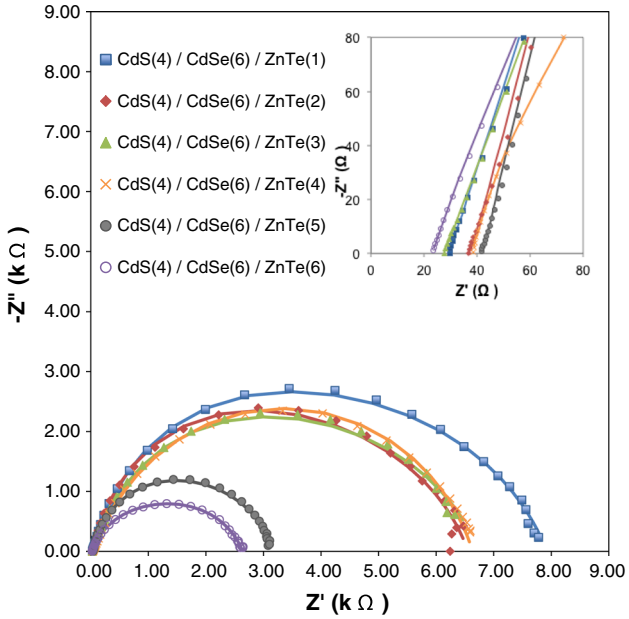

Fig. 12 Nyquist plots of CdS(4)/CdSe(6)/ZnTe(n) QDSSCs in dark with 0.45 V bias. Details of the plots at high frequencies are shown in the *inset*

Table 6 EIS results of CdS(4)/CdSe(6)/ZnSe(n) QDSSC in dark with 0.40 V bias: series resistance, charge-transfer resistance, impedance, and electron lifetime

Sample	R_S (Ω)	R_r (kΩ)	CPE2-T (μS s^n)	CPE2-P ($0 < n < 1$)	τ (ms)
CdS(4)/CdSe(6)/ZnSe(1)	23.56	2.09	4.87	0.92	6.92
CdS(4)/CdSe(6)/ZnSe(2)	25.86	2.60	5.18	0.90	8.24
CdS(4)/CdSe(6)/ZnSe(3)	32.29	2.76	5.00	0.91	8.81
CdS(4)/CdSe(6)/ZnSe(4)	26.03	2.74	4.15	0.92	7.69
CdS(4)/CdSe(6)/ZnSe(5)	20.74	2.03	6.54	0.95	10.77
CdS(4)/CdSe(6)/ZnSe(6)	29.30	1.10	22.20	0.94	19.21

lifetime, 74.87 ms is observed in CdS(4)/CdSe(6) QDSSC for which the efficiency is the highest.

The best performing CdS/CdSe QDSSCs with ZnSe and ZnTe as the passivation layers were further analyzed with EIS. For the batch of CdS(4)/CdSe(6)/ZnSe(n) QDSSCs, Nyquist plot results are shown in Fig. 11 and the EIS data are presented in Table 6. As more ZnSe layers are added on top of the CdS(4)/CdSe(6) QD structure, the charge-transfer resistance, R_r increases, indicating more resistive pathway for the electron to go through. However, the R_r for CdS(4)/CdSe(6)/ZnSe(6) QDSSC is substantially lower compared to the rest in the series. We do not rule out the possibility of enhanced photocurrent injection in the cell. Although the charge-transfer resistance is low, the calculated true chemical capacitance of this cell is high resulting in longer electron lifetime, 19.21 ms. This conforms well with the high efficiency of the cell as explained in the previous section. In general, the electron lifetime of the cell increased with more SILAR cycles used for the ZnSe deposition. This substantiates our hypothesis that ZnSe involves in photocurrent transport rather than as a passivation barrier.

In CdS(4)/CdSe(6)/ZnTe(n) QDSSC, the charge-transfer resistance, R_r observed is inconsistent with the number of SILAR cycles used for the deposition of ZnTe. In most cases, the R_r increased with the addition of ZnTe layers with the exception in the CdS(4)/CdSe(6)/ZnTe(6) QDSSC (refer Fig. 12; Table 7). This cell has a lower true chemical capacitance as well, which yields a low electron lifetime value. As a result, it has the worst performance within the batch. With the increase of ZnTe SILAR cycles, the electron lifetime reduced gradually signifying a faster electron recombination at the photoanode/electrolyte interface. It is perceived that there could be a band energy misalignment in the CdS(4)/CdSe(6)/ZnTe(n) cascade structure. As a

Table 7 EIS results of CdS(4)/CdSe(6)/ZnTe(n) QDSSCs in dark with 0.45 V bias: series resistance, charge-transfer resistance, impedance, and electron lifetime

Sample	R_S (Ω)	R_r (kΩ)	CPE2-T (μS s^n)	CPE2-P ($0 < n < 1$)	τ (ms)
CdS(4)/CdSe(6)/ZnTe(1)	29.12	2.27	7.71	0.99	16.74
CdS(4)/CdSe(6)/ZnTe(2)	37.15	2.32	5.68	1.00	13.18
CdS(4)/CdSe(6)/ZnTe(3)	27.38	1.79	8.28	0.96	12.38
CdS(4)/CdSe(6)/ZnTe(4)	37.99	3.50	8.82	0.80	12.86
CdS(4)/CdSe(6)/ZnTe(5)	42.07	2.22	12.53	0.81	11.67
CdS(4)/CdSe(6)/ZnTe(6)	22.99	0.99	20.34	0.80	7.53

result, charge transfer is hindered and charge recombination is preferred at the photoanode/electrolyte interface. As there is no significant improvement in electron lifetime, ZnTe is not suitable for either as a passivation layer or a photocurrent transporter.

4 Conclusions

Co-sensitized solar cells were prepared with CdS and CdSe QDs and optimized with respect to the number of SILAR cycles used for the QD deposition. The best performance was obtained with photoanode having CdS(4)/CdSe(6) structure. By passivating the QDs co-sensitized TiO_2 film with ZnS, an efficiency of 1.37 % was obtained. However, when the ZnS layer was replaced with ZnSe or ZnTe, there was no significant improvement in the solar cell performance. The lower performance of the cells with ZnSe or ZnTe passivation layer was due to higher charge-transfer resistance at the photoanode/electrolyte interface. Nevertheless, ZnSe has the potential to be applied as photocurrent transporter in a cascade QD structure as such cells have longer electron lifetime. ZnTe, on the other hand, is not recommended for the application in QDSSC as its implication is not that significant.

Acknowledgments The authors would like to thank the University of Malaya for the grants PV094-2012A and RP003-13AFR. H.K. Jun thanks University of Malaya for the Fellowship Scheme Scholarship.

References

1. Jun HK, Careem MA, Arof AK (2013) Quantum dot-sensitized solar cells—perspective and recent developments: a review of Cd chalcogenide quantum dots as sensitizers. Renew Sustain Energy Rev 22:148–167
2. Kamat PV (2008) Quantum dot solar cells. Semiconductor nanocrystals as light harvesters. J Phys Chem C 112:8735–18753
3. Ruhle S, Shalom M, Zaban A (2010) Quantum-dot-sensitized solar cells. ChemPhysChem 11:2290–2304
4. Chang C-H, Lee Y-L (2007) Chemical bath deposition of CdS quantum dots onto mesoscopic TiO_2 films for application in quantum-dots-sensitized solar cells. Appl Phys Lett 91:053503
5. Diguna LJ, Shen Q, Kobayashi J, Toyoda T (2007) High efficiency of CdSe quantum-dot-sensitized TiO_2 inverse opal solar cells. Appl Phys Lett 91:023116
6. Tubtimtae A, Wu K-L, Tung H-Y, Lee M-W, Wang GJ (2010) Ag_2S quantum dot-sensitized solar cells. Electrochem Commun 12:1158–1160
7. Feng J, Han J, Zhao X (2009) Synthesis of $CuInS_2$ quantum dots on TiO_2 porous films by solvothermal method for absorption layer of solar cells. Prog Org Coat 64:268–273
8. Plass R, Pelet S, Krueger J, Gratzel M, Bach U (2002) Quantum dot sensitization of organic–inorganic hybrid solar cells. J Phys Chem B 106:7578–7580
9. Park N-G (2013) Organometal perovskite light absorbers toward a 20% efficiency low-cost solid-state mesoscopic solar cell. J Phys Chem Lett 4:2423–2429
10. Ruhle S, Yahav S, Greenwald S, Zaban A (2012) Importance of recombination at the TCO/electrolyte interface for high efficiency quantum dot sensitized solar cells. J Phys Chem C 116: 17473–17478
11. Tachan Z, Hod I, Shalom M, Grinis L, Zaban A (2013) The importance of the TiO_2/quantum dots interface in the recombination processes of quantum dot sensitized solar cells. Phys Chem Chem Phys 15:3841–3845
12. Shen Q, Kobayashi J, Diguna LJ, Toyoda T (2008) Effect of ZnS coating on the photovoltaic properties of CdSe quantum dot-sensitized solar cells. J Appl Phys 103:084304
13. de la Fuente MS, Sanchez RS, Gonzalez-Pedro V, Boix PP, Mhaisalkar SG, Rincon ME, Bisquert J, Mora-Sero I (2013) Effect of organic and inorganic passivation in quantum-dot-sensitized solar cells. J Phys Chem Lett 4:1519–1525
14. Tachibana Y, Umekita K, Otsuka Y, Kuwabata S (2008) Performance improvement of CdS quantum dots sensitized TiO_2 solar cells by introducing a dense TiO_2 blocking layer. J Phys D Appl Phys 41:102002
15. Lee HJ, Wang M, Chen P, Gamelin DR, Zakeeruddin SM, Gratzel M, Nazeeruddin MK (2009) Efficient CdSe quantum dot-sensitized solar cells prepared by an improved successive ionic layer adsorption and reaction process. Nano Lett 9:4221–4227
16. Jun HK, Careem MA, Arof AK (2013) A suitable electrolyte for CdSe quantum dot-sensitized solar cells. Int J Photoenergy 2013:942139
17. Toyoda T, Sato J, Shen Q (2003) Effect of sensitization by quantum-sized CdS on photoacoustic and photoelectrochemical current spectra of porous TiO_2 electrodes. Rev Sci Instrum 74:297–299
18. Barcelo I, Lana-Villarreal T, Gomez R (2011) Efficient sensitization of ZnO nanoporous films with CdSe grown by successive ionic layer adsorption and reaction (SILAR). J Photochem Photobiol A Chem 220:47–53
19. Wang X, Koleilat GI, Tang J, Liu H, Kramer IJ, Debnath R, Brzozowski L, Barkhouse DAR, Levina L, Hoogland S, Sargent

EH (2011) Tandem colloidal quantum dot solar cells employing graded recombination layer. Nat Photonics 5:480–484
20. Gratzel M (2001) Photoelectrochemical cells. Nature 414(2001): 338–344
21. Bang JH, Kamat PV (2009) Quantum dot sensitized solar cells. A tale of two semiconductor nanocrystals: CdSe and CdTe. ACS Nano 3:1467–1476
22. Jun HK, Careem MA, Arof AK (2014) Fabrication, characterization, and optimization of CdS and CdSe quantum dot-sensitized solar cells with quantum dots prepared by successive ionic layer adsorption and reaction. Int J Photoenergy 2014:939423
23. Seo M-H, Hwang W-P, Kim Y-K, Lee J-K, Kim M-R (2011) Improvement of quantum dot-sensitized solar cells based on Cds and CdSe quantum dots. In: 37th IEEE photovoltaic specialists conference (PVSC), pp 002652–002655
24. Zhang Y, Zhu J, Yu X, Wei J, Hu L, Dai S (2012) The optical and electrochemical properties of CdS/CdSe co-sensitized TiO_2 solar cells prepared by successive ionic layer adsorption and reaction processes. Sol Energy 86:964–971
25. Lee HJ, Bang J, Park J, Kim S, Park S-M (2010) Multilayered semiconductor (CdS/CdSe/ZnS)-sensitized TiO_2 mesoporous solar cells: all prepared by successive ionic layer adsorption and reaction processes. Chem Mater 22:5636–5643
26. Tian J, Gao R, Zhang Q, Zhang S, Li Y, Lan J, Qu X, Cao G (2012) Enhanced performance of CdS/CdSe quantum dot co-sensitized solar cells via homogeneous distribution of quantum dots in TiO_2 film. J Phys Chem C 116:18655–18662
27. Li Z-X, Xie Y-L, Xu H, Wang T-M, Xu Z-G, Zhang H-L (2011) Expanding the photoresponse range of TiO_2 nanotube arrays by CdS/CdSe/ZnS quantum dots co-modification. J Photochem Photobiol A Chem 224:25–30
28. Chen J, Wu J, Lei W, Song JL, Deng WQ, Sun XW (2010) Co-sensitized quantum dot solar cell based on ZnO nanowire. Appl Surf Sci 256:7438–7441
29. Hossain MA, Jennings JR, Shen C, Pan JH, Koh ZY, Matthews N, Wang Q (2012) CdSe-sensitized mesoscopic TiO_2 solar cells exhibiting >5% efficiency: redundancy of CdS buffer layer. J Mater Chem 22:16235–16242
30. Fang S-Q, Kim D, Kim J–J, Jung DW, Kang SO, Ko J (2009) Highly efficient CdSe quantum-dot-sensitized TiO_2 photoelectrodes for solar cells applications. Electrochem Commun 11: 1337–1339
31. Yu X-Y, Lei B-X, Kuang D-B, Su C-Y (2012) High performance and reduced charge recombination of CdSe/CdS quantum dot-sensitized solar cells. J Mater Chem 22:12058
32. Gonzalez-Pedro V, Xu X, Mora-Sero I, Bisquert J (2010) Modeling high-efficiency quantum dot sensitized solar cells. ACS Nano 4:5783–5790
33. Wang Q, Moser J-E, Gratzel M (2005) Electrochemical impedance spectroscopy analysis of dye-sensitized solar cells. J Phys Chem B 109:14945–14953
34. Fabregat-Santiago F, Bisquert J, Garcia-Belmonte G, Boschloo G, Hagfeldt A (2005) Influence of electrolyte in transport and recombination in dye-sensitized solar cells studied by impedance spectroscopy. Sol Energ Mater Sol C 87:117–131
35. Meng K, Surolia PK, Byrne O, Thampi KR (2014) Efficient CdS quantum dot sensitized solar cells made using novel Cu_2S counter electrode. J Power Sources 248:218–223
36. Fabregat-Santiago F, Garcia-Belmonte G, Bisquert J, Zaban A, Salvador P (2002) Decoupling of transport, charge storage, and interfacial charge transfer in the nanocrystalline TiO_2/electrolyte system by impedance methods. J Phys Chem B 106:334–339